Genes & Diseases (2023) 10, 2586–2596

Available online at www.sciencedirect.com

ScienceDirect

journal homepage: www.keaipublishing.com/en/journals/genes-diseases

FULL LENGTH ARTICLE

A novel *in vitro* prognostic model of bladder cancer based on urine-derived living tumor cells

Jiaqi Wang [a,b,1], Jiying Zhu [a,c,1], Junchi Hu [d,1], Ziruoyu Wang [a,1], Xiaobo Wang [a], Jianbo Pan [d], Yiwei Chu [b], Zengxia Li [a], Wei Jiang [a], Chunmin Liang [c,*], Jun Hou [e,], Jianming Guo [f,***], Yongjun Dang [a,d,****], Shuai Jiang [f,g,*****]**

[a] *Key Laboratory of Metabolism and Molecular Medicine, Ministry of Education and Department of Biochemistry and Molecular Biology, School of Basic Medical Sciences, Fudan University, Shanghai 200032, China*
[b] *Department of Immunology, School of Basic Medical Sciences, Fudan University, Shanghai 200032, China*
[c] *Laboratory of Tumor Immunology, Department of Anatomy, Histology, and Embryology, School of Basic Medical Sciences, Fudan University, Shanghai 200032, China*
[d] *Center for Novel Target and Therapeutic Intervention, Chongqing Medical University, Chongqing 400016, China*
[e] *Department of Pathology, Zhongshan Hospital, Fudan University, Shanghai 200032, China*
[f] *Department of Urology, Zhongshan Hospital, Fudan University, Shanghai 200032, China*
[g] *Department of Urology, Zhongshan Hospital Wusong Branch, Fudan University, Shanghai 200940, China*

Received 17 May 2022; received in revised form 28 August 2022; accepted 22 October 2022
Available online 26 November 2022

***** Corresponding author. Department of Urology, Zhongshan Hospital, Fudan University, 180 Fenglin Road; Department of Urology, Zhongshan Hospital Wusong Branch, Fudan University, 216 Mudanjiang Road, Shanghai 200032, China.
**** Corresponding author. Center for Novel Target and Therapeutic Intervention, Chongqing Medical University, 1 Medical School Road, Yuzhong District, Chongqing 400016, China.
*** Corresponding author. Department of Urology, Zhongshan Hospital, Fudan University, 180 Fenglin Road, Shanghai 200032, China.
** Corresponding author. Department of Pathology, Zhongshan Hospital, Fudan University, 180 Fenglin Road, Shanghai 200032, China.
* Corresponding author. Laboratory of Tumor Immunology, Department of Anatomy, Histology and Embryology, School of Basic Medical Sciences, Shanghai Medical College, Fudan University, 131 Dongan Road, Shanghai 200032, China.
E-mail addresses: cmliang@fudan.edu.cn (C. Liang), hou.jun@zs-hospital.sh.cn (J. Hou), guo.jianming@zs-hospital.sh.cn (J. Guo), yongjundang@fudan.edu.cn, yjdang@cqmu.edu.cn (Y. Dang), jiang.shuai@zs-hospital.sh.cn (S. Jiang).
Peer review under responsibility of Chongqing Medical University.
[1] These authors contributed equally to this work.

https://doi.org/10.1016/j.gendis.2022.10.022

KEYWORDS
Bladder cancer;
Immune checkpoint inhibitors;
Predictive model;
Primary cells;
Urine

Abstract Bladder cancer (BLCA) remains a difficult malignancy to manage because of its high recurrence, intense follow-up, and invasive diagnostic and treatment techniques. Immune checkpoint inhibitors (ICIs) have forged a new direction for the treatment of BLCA, but it is currently challenging to predict whether an individual patient will be sensitive to ICIs. We collected 43 urine/tumor samples from BLCA patients for primary bladder cancer cells (BCCs) culturing using our previously reported BCC culture platform. We used flow cytometry (FCM) to measure the expression levels of Programmed Death-Ligand 1 (PD-L1) on BCCs before and after interferon-gamma (IFN-γ) treatment and found that PD-L1 expression and the sensitivities to IFN-γ varied among patients. RNA-sequencing, western blotting, and programmed death-1 (PD-1) binding assays confirmed that the BCC FCM-based PD-L1 detection platform (BC-PD-L1) was reliable and was not hindered by the glycosylation of PD-L1. In the subsequent retrospective study, we found that IFN-γ-stimulated PD-L1 (sPD-L1) expression on BCCs detected by BC-PD-L1 could predict the prognosis of BLCA patients. Importantly, the prognostic value was similar or even better in urine-derived BC-PD-L1 (UBC-PD-L1). Transcriptome analysis showed that BCCs with high sPD-L1 tended to enrich genes associated with the collagen-containing extracellular matrix, cell—cell adhesion, and positive regulation of the immune system. In addition, the UBC-PD-L1 also exhibited predictive value for ICI response in BLCA patients. In conclusion, as a novel personalized urine-detection method, UBC-PD-L1 may provide a rapid, accurate, and non-invasive tool for monitoring tumor progression, predicting therapeutic responses, and helping improve BLCA clinical treatment in future.

Introduction

Bladder cancer (BLCA) is among the most expensive cancers to manage from diagnosis to death. For non-muscle invasive bladder cancer (NMIBC), the cost is due to the frequent disease recurrence (as high as 80%), intense follow-up, and expensive, invasive techniques for diagnosis and treatment.[1,2] Meanwhile, muscle-invasive bladder cancer (MIBC) represents an aggressive disease probably with rapid progression to metastases and poor overall survival despite intensive local and systemic therapy.[3] Checkpoint blockade immunotherapy has been a significant clinical advance for nearly all cancers. For BLCA, immune checkpoint inhibitors (ICIs) are gradually displacing previous treatment regimens as first- and second-line therapies. However, their objective response rates (ORRs) are unsatisfactory, and there is a lack of reliable predictors in clinical practice.[4] Thus, prognostic and predictive models with high discriminative accuracy are urgently needed to facilitate the individual decision-making process and improve clinical outcomes for BLCA patients.

Cystoscopy, although generally accepted as the gold standard for BLCA detection and surveillance, is an invasive and expensive procedure. These invasive tests can lead to urinary tract infections, discomfort, or injury, leading to a patient's discontinuation of follow-up.[5] Therefore, noninvasive assays with high specificity, high sensitivity, and moderate cost would be greatly beneficial. Liquid biopsies have been proven to provide equally accurate and dynamic clinical information and can capture the complex genetic mutations of profiles of primary and metastatic tumors.[6] Urine is the most convenient source of liquid biopsies for BLCA. It is non-invasive, easy to handle, and suitable for real-time monitoring. Indeed, urine has been extensively explored for clinical diagnosis and monitoring of BLCA by detecting markers, such as circulating cell-free DNA, microRNA, circular RNA, non-coding RNA, proteins, cells *etc*.[7—10] Novel tests such as UriFind, PredicineBEACONTM, and Visiocyt emerge in endlessly, while there are few studies focused on the characteristics of urinary exfoliated tumor cells.[11,12]

We previously reported a method to generate continuous primary cell cultures by the conditional reprogramming (CR) technique from urine samples of BLCA patients.[13] The CR technique has proven useful for basic and clinical research on many kinds of cancers, including drug research and personalized medicine.[14] In our previous study, we validated that urine-derived bladder cancer cells (U-BCCs) capture the complex molecular characteristics of primary and metastatic tumors, as well as rare mutations below detection limits in the clinic, and confirmed their potential use in therapeutic prediction. Here, we explore other potential applications of this urine-derived model in BLCA, with the goal of facilitating better clinical management of this common malignant tumor.

Materials and methods

Patients and specimens

All recruited patients were confirmed with BLCA by pathology. This study has been approved by Zhongshan Hospital Ethics Committee (project number: B2019-330R). Urine and tumor samples were collected after obtaining informed consent from the patients. All experimental

protocols were carried out in accordance with the guidelines approved by the Zhongshan Hospital Ethics Committee. Tissue microarrays (TMAs) were constructed using archived pathological formalin-fixed, paraffin-embedded (FFPE) specimens. Patients' clinical data were retrospectively collected from the Zhongshan hospital electronic patient record system.

Urine and tissue processing

Urine samples were collected from the clean, mid-stream urine of patients. 50 mL of urine was collected in sterile tubes with penicillin/streptomycin mix (final concentration: 200 U/mL penicillin and 200 μg/mL streptomycin) and centrifuged at 1000 rpm for 10 min. The supernatant was aspirated, and the pellet was washed with phosphate-buffered saline (PBS) three times before being added to culture plates.

Bladder tumor tissues were collected from patients during surgery and then transferred into a 15 mL tube with sterilized PBS. All samples were packaged on ice and the following steps were conducted in sterile conditions within 6 h. Tissues were minced with scalpels into small pieces and digested with a digestion buffer composed of dispase (Gibco), collagenase (Sigma), and hyaluronidase (Sigma). After dissociation, the cells were centrifuged at 1,000 rpm for 5 min and the supernatant was discarded. Cell pellets were re-suspended in a medium and transferred into plates for culturing.

Establishment of urine and tumor primary bladder cancer cells

For the preparation of complete F medium, we mixed 373 mL of DMEM (Gibco) and 125 mL of F12 nutrient (Gibco) and added the following additions with final concentrations of 5 μg/mL insulin (Sigma-Aldrich), 0.125 ng/mL EGF (Sangon) and 25 ng/mL hydrocortisone (Sigma-Aldrich). The solution was filtered with a 0.2-μm sterile filter and stored at 4°C for up to 2 weeks after adding the ROCK inhibitor Y-27632 (DC Chemicals) at a final concentration of 10 μM. NIH-3T3 cells were irradiated at a dose of 50 Gy as feeder cells. Cell pellets derived from urine and tumor samples were transferred into a culture dish with feeder cells at a confluence of 1×10^4 cells/cm^2 in a complete F medium. The formation of visible BCC colonies was monitored 24—72 h after seeding. BCCs were differentially trypsinized to separate from feeder cells and passaged when reached 80%—90% confluency using a 1:3 dilution and were given fresh medium every 2—3 days.

Programmed death-ligand 1 (PD-L1) expression detection of BCCs by flow cytometry (FCM)

BCCs were harvested by dissociation with 0.25% trypsin and washed with PBS. Then cells were counted, resuspended in PBS added with APC anti-human CD274 (Biolegend), and incubated on ice for 15—20 min in the dark. After washing twice with PBS, cell-surface PD-L1 expression was detected by FCM using the iQue screener plus (IntelliCyt).

To assess the induced expression of PD-L1 by Interferon-gamma (IFN-γ), BCCs were seeded at a 6-well plate for 1×10^5 cells/well and treated with recombinant IFN-γ (100 IU/mL, R&D systems) for 24 h. Then the cells were harvested for PD-L1 expression detection by FCM as described above. Data are represented both as normalized mean fluorescence intensity (MFI) and positive percentage.

Programmed Death-1 (PD-1) binding ability detection of BCCs by FCM

BCCs were harvested and washed with PBS. After centrifugation, cells were resuspended in 50 μL PBS at a concentration of 1×10^7 cells/mL and incubated with 50 ng/μL recombinant human PD-1-Fc protein for 30 min at room temperature. Then cells were washed twice with PBS and stained with FITC conjugated anti-Human IgG antibody (Abcam) at 4 °C for 30 min in the dark. After washing with PBS, the cell surface fluorescence was analyzed by iQue screener plus (IntelliCyt). Background fluorescence was estimated by the same samples that were not incubated with recombinant human PD-1-Fc protein. For IFN-γ stimulation, BCCs were first treated with IFN-γ (100 IU/mL) for 24 h and then were harvested for PD-1 binding ability detection by FCM as described above.

RNA-sequencing (RNA-seq)

Total RNA was extracted using Trizol (Invitrogen) according to the manufacturer's instructions. The qualified RNAs were treated with DNase (5 U/μL) (TaKaRa) at 37 °C for 30 min. Then the DNase-treated RNAs were purified by Dynabeads® Oligo (dT)25 (Life). Libraries were prepared from ~500 ng of total RNA with NEBNext® UltraTM RNA Library Prep Kit for Illumina following the manufacturer's directions. Paired-end 150 bp sequencing was performed on Illumina Novaseq according to the manufacturer's directions. RNA-Seq data quality was assessed with the FastQC (version 0.11.7) software before any data filtering criteria were applied. Reads were mapped to the human reference genome (GRCh38 assembly) by using HISAT2 software (v2.2.0).[15] After mapping, mouse genes were filtered out using XenofilteR (v1.6) R packages.[16] The mapped reads were assembled into transcripts or genes by using StringTie software (v2.1.2)[17] and the genome annotation file (EMBL_Homo_sapiens.GRCh38.101.gtf). The expression profiles were normalized by TPM (transcripts per million) method.

The relative abundance of the transcript was normalized by R package DESeq2 (v1.34.0).[18] DEGs were identified using DESeq2 by comparing high IFN-γ-stimulated PD-L1 (sPD-L1) against low sPD-L1 samples sequenced together. Genes with P value < 0.05 and $\log_2$FoldChange ≥ 1.0 by DESeq2 were defined as up-regulated DEGs; genes with P value < 0.05 and $\log_2$FoldChange ≤ -1.0 were defined as down-regulated DEGs.

Over-Representation Analysis (ORA) of DEGs in Gene Ontology (GO) used by the R package clusterProfiler (v4.2.2).[19] In addition, Gene Set Enrichment Analysis (GSEA)-based[20] GO analyses was also conducted by the

clusterProfiler (v4.2.2) to explore differential enrichment pathways between high- and low-sPD-L1 samples. Normalized enrichment score was acquired using gene set permutations with 1000 times and the cutoff *P* value was set as 0.05 for filtering the significant enrichment results.

Western blot analysis

Cells were pelleted, washed with PBS, and then lysed with Radio Immunoprecipitation Assay Lysis (RIPA) buffer (Thermo Scientific) supplemented with protease inhibitor cocktail (CST). Protein concentration was determined by the BCA Protein assay kit (Thermo Scientific) and lysates were then boiled for 10 min. Proteins were separated by sodium dodecyl sulfate-polyacrylamide gel electrophoresis (SDS-PAGE) and transferred onto a nitrocellulose membrane (Pall). Membranes were blocked for 1 h at room temperature with 5% milk in 1 × Phosphate Buffered Saline Tween-20 (PBST) and incubated with the indicated primary antibodies at 4 °C overnight. After washing with PBST three times for 30 min, membranes were incubated with secondary antibodies at room temperature for 1 h. The membranes were washed with PBST three times and visualized with chemiluminescence (CLiNX). Antibodies against the following human proteins were used: GAPDH (SCB), PD-L1 (Yurogen), PD-L1 E1L3N (CST), and PD-L1 28-8 (Abcam). Band intensities were quantified by ImageJ and were normalized using GAPDH as a housekeeping protein. Results are representative of three independent experiments.

Tissue microarray and immunohistochemistry

TMAs were created using a manual tissue microarrayer (Beecher Instruments). Each marked block was sampled twice with a core diameter of 1.0 mm arrayed in a rectangular pattern with 1.0 mm between the centers of each core, creating a duplicate TMA layout. Hematoxylin and eosin (H&E) staining and immunohistochemical (IHC) staining were done on FFPE 4-μm sections of the TMA. Slides were deparaffinized in xylene and rehydrated through graded concentrations of ethanol to distilled water. Antigen retrieval was performed with 10 mM citric acid buffer (pH 6.0) for 10 min in a high-pressure cooker. Endogenous peroxidase activity was blocked by incubation with 3% H_2O_2 for 10 min at room temperature. Slides were subsequently blocked with a blocking buffer for 1 h at room temperature. Slides were incubated overnight with primary antibodies against PD-1 (Abcam) and PD-L1 (Abcam) at 4 °C. After washing with PBS, the slides were incubated with horseradish peroxidase-conjugated secondary antibody at room temperature for 30 min. Finally, antibodies were visualized using 3,3′-diaminobenzidine (DAB) chromogen, counterstained with hematoxylin, and mounted with DPX (Sigma-Aldrich).

To evaluate the density of positively stained cells, three respective areas of stroma and tumor core were evaluated at 200 × magnification and the mean value was adopted. Two pathologists (Jun Hou and Yuan Shi) were blinded to the clinicopathologic data and scored all samples independently. The mean score was adopted.

Statistical analysis

Disease-free survival (DFS) is defined as the time from the date of obtaining samples to either local recurrence and progression (defined as disease recurrence or progression within the bladder) or development of metastatic disease (disease recurrence or progression outside the bladder) based on computed tomography (CT) or cystoscope results. Overall survival (OS) implies the length of time from the date of obtaining samples to death from any cause. Kaplan–Meier curves were used to plot the survival data. The curves between DFS and OS were statistically compared using the log-rank test. Data were censored if patients were free of recurrence/progression or alive at the last follow-up.

Correlation analyses were computed using Spearman's rank correlation coefficient test. All tests were two-sided, and statistical significance was set at $P < 0.05$. The difference between the two groups was evaluated with unpaired *t*-test. All statistical analyses were performed using GraphPad Prism 9 software.

Results

PD-L1 expression and the response to IFN-γ detected by BC-PD-L1 varied in different BCCs

We collected urine ($n = 26$) and tumor ($n = 17$) samples from 43 BLCA patients for primary cell culturing, detected expression levels of PD-L1 on the cell surface before and after IFN-γ treatment by BCCs FCM-based PD-L1 detection platform (BC-PD-L1) and confirmed the prognostic and predictive value of urine-derived BC-PD-L1 (UBC-PD-L1) in clinical practice (Fig. 1A, B). Detailed patient information was summarized in Table S1. The enrolled patients included 79.1% (34/43) of males and 20.9% (9/43) of females. NMIBC and MIBC accounted for 46.5% (20/43) and 53.5% (23/43), respectively, among which 65.1% (28/43) were primary, and 34.9% (15/43) were recurrent (Fig. 1B). FCM analysis showed that PD-L1 was constitutively expressed at various levels on different BCCs, from extremely low expression (e.g., patients 14 and 44) to very high expression (e.g., patients 32 and 36) (Fig. 1C). IFN-γ plays a key role in the activation of cellular immunity and subsequently, the stimulation of antitumor immune response; it is known to upregulate PD-L1 expression on a variety of cell types.[21] As expected, PD-L1 expression was upregulated in almost all BCCs after incubation with 100 IU/mL IFN-γ for 24 h (Fig. 1C). Interestingly, the fold change of PD-L1 expression levels after IFN-γ stimulation varied largely among different BCCs and exhibited a relatively negative correlation with basal PD-L1 expression levels on BCCs (****$P < 0.0060$, $r = -0.4125$) (Fig. S1A, B). As MFI represents the average level of the cell population, we also analyzed the proportion of PD-L1 positive cells in detail. The proportions of PD-L1 positive cells in BCCs before and after IFN-γ stimulation also varied widely between patients, ranging from a low percentage to greater than 90% (Fig. S1C). Moreover, the PD-L1 positive percentage was significantly positively correlated with PD-L1

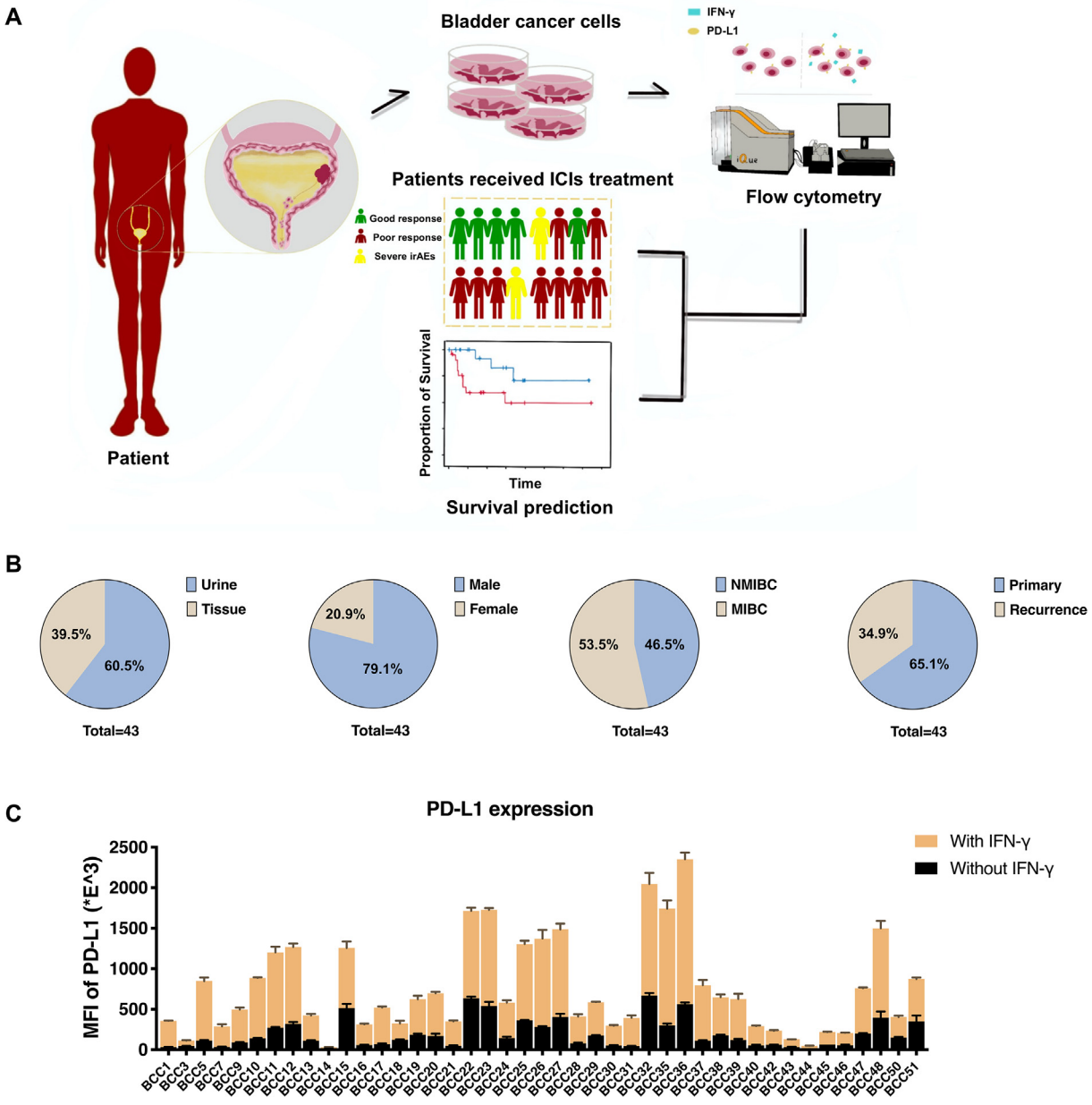

Figure 1 Overview of establishment of BC-PD-L1. **(A)** Overview of the models of BCCs for potential applications in prediction of prognosis in bladder cancer. Urine/tumor samples were collected from BLCA patients for primary bladder cancer cell culturing. PD-L1 expression levels of BCCs before and after IFN-γ stimulation were measured by FCM and used for prognosis and ICI response prediction. **(B)** Pie charts showing the classification of all urine/tumor-provided patients based on sample source, gender, pathology group, and disease status. **(C)** Levels of PD-L1 expression on BCC cell surface before and after IFN-γ treatment measured by FCM analysis. (MFI mean ± standard deviation). MFI, median fluorescence intensity.

expression before IFN-γ stimulation (****$P < 0.0001$, $r = 0.8225$), while the two indicators showed moderately positive correlation after IFN-γ stimulation (**$P = 0.0047$, $r = 0.4230$) (Fig. S1D, E), indicating that even in PD-L1 positive cells, the expression levels of PD-L1 on the surface of individual cells differ. We also collected both urine and tumor samples from four patients. Paired U/T-BCCs exhibited similar sPD-L1 expression levels in patient 1, 3, and 5, while in patient 7, U-BCC showed a lower sPD-L1 level than T-BCC (Fig. S1F). Further analysis revealed that in patients 1, 3, and 7, MKI67 was higher expressed on U-BCCs compared to T-BCCs, indicating a higher proliferative index in U-BCCs (Fig. S1G).

BC-PD-L1 is reliable and can avoid the hindrance of the heavy glycosylation of PD-L1

To verify the reliability of BC-PD-L1, we performed RNA-seq on BCCs and demonstrated a moderately positive correlation between PD-L1 MFI levels and PD-L1 mRNA levels (****$P < 0.0001$, $r = 0.5864$) (Fig. S2A). We further used

western blotting to re-detect protein levels of PD-L1 expression on some randomly selected BCCs. BCC3, BCC22, BCC9, and BCC21 were examined both before and after IFN-γ treatment. Previous studies reported that PD-L1 is a highly glycosylated protein. Consistent with this, PD-L1 was proved to be highly glycosylated in all detected BCCs whether stimulated by IFN-γ or not (Fig. 2A; Fig. S2B). Quantified results of western blotting by ImageJ were significantly positively correlated with the corresponding PD-L1 level detected by FCM (***$P = 0.0001$, $r = 0.8861$) (Fig. 2A), indicating that the BC-PD-L1 can avoid hindering by the heavy glycosylation of PD-L1. Notably, the BC-PD-L1 can detect more comprehensive PD-L1 glycosylation and non-glycosylation patterns than clinically used IHC antibodies (Fig. S2B).

Considering glycosylation is required for the PD-L1 and PD-1 interaction, we further employed an *in vitro* receptor-ligand binding assay to investigate the interaction between PD-L1 on BCCs and PD-1 ligands. The PD-1 binding abilities of BCCs were measured by incubating with recombinant

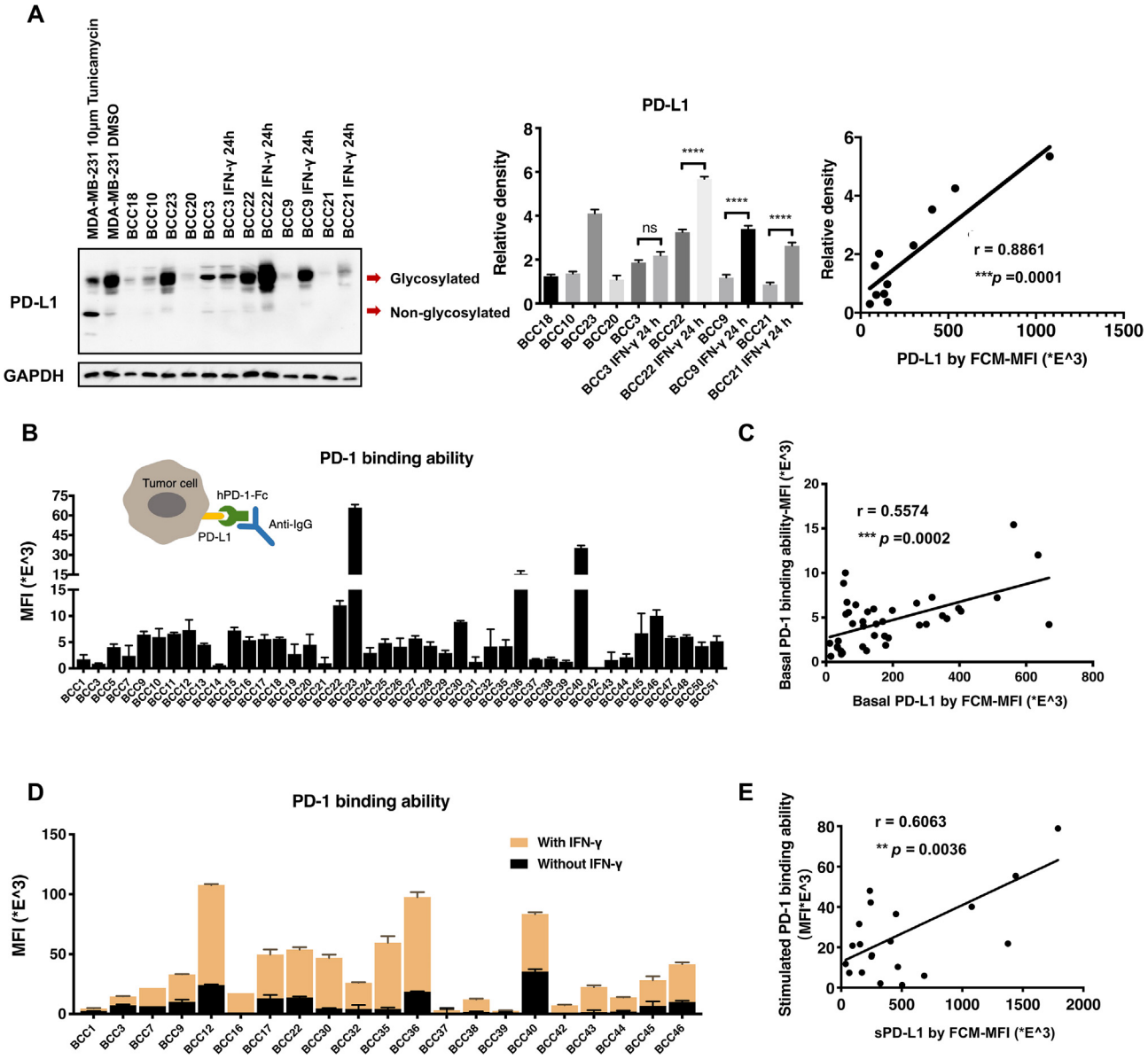

Figure 2 Reliability verification of BC-PD-L1. **(A)** Western blot analysis of PDL1 expression on BCCs with or without IFN-γ treatment (left). Quantification of the western blotting data. The significance of the value is indicated by asterisks (*). ****$P < 0.0001$ (middle). Correlation analysis of the PD-L1 expression levels on BCCs detected by FCM and Western blot (right). **(B)** Levels of PD-1 binding abilities of BCCs detected by FCM (MFI mean ± standard deviation). Top left: Diagram of BCC binding abilities to PD-1 protein detected by FCM. BCCs were incubated with recombinant human PD-1-Fc protein for 30 min and then stained with FITC-conjugated anti-Human IgG antibody for FCM. **(C)** Correlation analysis between PD-1 binding abilities and PD-L1 expression levels of BCCs. **(D)** Levels of PD-1 binding abilities of BCCs before and after IFN-γ treatment detected by FCM (MFI mean ± standard deviation). **(E)** Correlation analysis between IFN-γ-stimulated PD-1 binding abilities and IFN-γ-stimulated PD-L1 expression levels of BCCs.

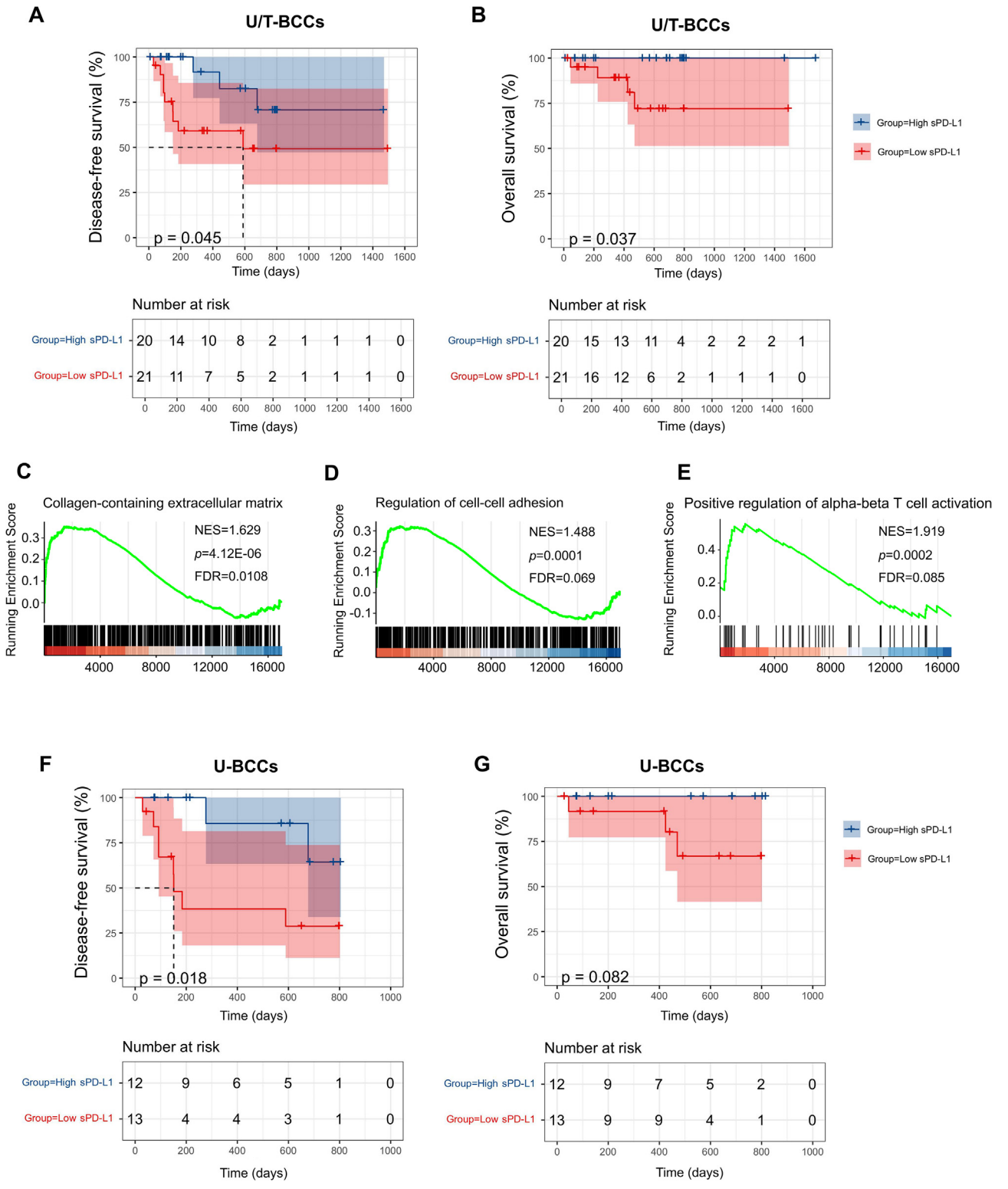

Figure 3 BC-PD-L1 showed survival prediction value in BLCA. **(A)** Kaplan–Meier plots of DFS curve of urine/tumor-derived BCCs (U/T-BCCs) with high and low sPD-L1 expression levels. **(B)** Kaplan–Meier plots of OS curve of urine/tumor-derived BCCs with high and low sPD-L1 expression levels. **(C–E)** GSEA was applied to determine the pathways enriched in high sPD-L1 BCCs in contrast to low sPD-L1 BCCs. **(F)** Kaplan–Meier plots of DFS curve of UBCCs with high and low sPD-L1 expression levels. **(G)** Kaplan–Meier plots of OS curve of U-BCCs with high and low sPD-L1 expression levels.

human PD-1-Fc protein and then subjected to IgG antibody for FCM (Fig. 2B). We validated the PD-1 binding detection platform using unmodified CHO-K1 cells and recombinant CHO-K1 cells that constitutively expressed human PD-L1 (CHO-K1-PD-L1) (Fig. S2C, D). As with PD-L1 expression, we observed clear differences in the PD-1 binding abilities of different BCCs before and after IFN-γ stimulation (Fig. 2B, D). There was a significant, moderately positive correlation between the PD-1 binding abilities and PD-L1 expression levels of BCCs both before and after IFN-γ stimulation (Fig. 2C, E), further validating the reliability of the BC-PD-L1.

BC-PD-L1, especially UBC-PD-L1, can predict the prognosis of BLCA patients

The prognostic role of PD-L1 in bladder cancer has been investigated in previous studies, but the results remain inconclusive. We retrospectively analyzed The Cancer Genome Atlas (TCGA) BLCA dataset ($n = 400$) by the patient clinical data and the corresponding PD-L1 mRNA expression levels. As with previously reported, no statistically significant prognostic value of transcriptional PD-L1 was observed in DFS ($P = 0.95$) and OS in BLCA ($P = 0.22$) (Fig. S3A, B). Then, we collected 85 archived pathological FFPE specimens from Zhongshan hospital to construct TMA and evaluated PD-L1 expression by IHC. Positive PD-L1 expression was detected in 24 (28.2%) samples and the rest were all negative. There was also no significant correlation between IHC-based PD-L1 expression and DFS ($P = 0.49$) or OS ($P = 0.65$) (Fig. S3C, D). Previous studies have reported that IFN-γ plays a pivotal role in antitumor host immunity.[21] As a downstream factor in the IFN-γ signaling pathway, sPD-L1 is capable of reflecting the response of tumor cells to IFN-γ to some extent. To explore the prognostic significance of sPD-L1 expression detected by BC-PD-L1, we collected follow-up information from the 43 patients. Kaplan—Meier analysis revealed that patients whose BCCs had higher sPD-L1 exhibited significantly longer DFS ($^{*}P = 0.045$) and OS ($\overline{\circ}P = 0.037$) (Fig. 3A, B). Next, we performed RNA-seq analysis on BCCs. Dimensionality reduction using principal component analysis (PCA) revealed that there were no significant differences between high and low sPD-L1 BCCs in the overall transcriptional profile (Fig. S4A). As shown in the volcano plot, there were 833 differentially expressed genes ($P < 0.05$, fold change >2) between high and low sPD-L1 BCCs groups (Fig. S4B). GSEA revealed that the collagen-containing extracellular matrix pathway was significantly up-regulated in high sPD-L1 BCCs, as with the related pathways associated with extracellular matrix (ECM), collagen trimer, and collagen binding (Fig. 3C; Fig. S4C—E). Collagen is the most significant component of the ECM and has been appreciated as a key driver for cancer progression. In keeping with this finding, the pathway of regulation of cell—cell adhesion, cell adhesion molecule production, and negative regulation of epithelial cell migration were also significantly down-regulated in low sPD-L1 BCCs (Fig. 3D; Fig. S4F—H). Moreover, enrichment of T cell activation, positive regulation of immune system process, and antigen processing in high sPD-L1 BCCs suggested that these tumors were "hotter" than low sPD-L1 groups, further implying their better survival (Fig. 3E; Fig. S4I—K).

Surprisingly, we found that U-BCCs also demonstrated similar or even better prognostic value for DFS and OS in BLCA patients (Fig. 3F, G). These findings implied that UBC-PD-L1 is more likely to be a potential prognostic model for clinical application in BLCA management in consideration of its non-invasive and convenient characteristics. We will continue to expand our sample size to further validate the biological characteristics of U-BCCs and support their clinical application.

UBC-PD-L1 exhibited predictive value for ICIs response in BLCA patients

Among 43 patients enrolled, eight patients received ICIs treatment. Urine samples were collected, as tumor tissues were not available from these advanced patients. We retrospectively analyzed the correlation between the results of UBC-PD-L1 and the clinical ICI response in these patients. As expected, UBC-PD-L1 results showed that ultra-high sPD-L1 levels were associated with severe immune-related adverse events (irAEs) after ICI treatment, moderate sPD-L1 levels were associated with a good response (partial response, PR), and ultra-low sPD-L1 levels were associated with no response (progressive disease, PD) (Fig. 4A, B). To be specific, CT of the BCC1, BCC31, BCC40, and BCC42 (ultra-low sPD-L1) patients showed PD after several months of ICI treatment. Positron emission tomography (PET)-CT of the BCC39 (moderate sPD-L1) patient showed the disappearance of lymph node metastasis and regression of primary tumor (PR) after 3 months of ICI treatment. CT of BCC47 (moderate sPD-L1) patient showed primary tumor regression (PR) after three months of ICI treatment. The BCC22 (ultra-high sPD-L1) patient received ICI treatment only once and presented severe irAEs (ataxia). The BCC9 (moderate sPD-L1) patient was the only inconsistent sample who received ICI treatment only once and developed severe irAEs (severe liver injury), probably due to his liver metastases (Fig. 4C). We indeed found that the UBC-PD-L1 exhibited better predictive value than IHC-based PD-L1 readouts in our study (Fig. 4A; Fig. S5). Taken together, our results suggest that the easy-to-use UBC-PD-L1 may provide a novel tool that enables doctors to distinguish patients who are most suitable for ICI treatment. We also need to continue to expand the sample size to further validate its clinical application.

Discussion

Bladder cancer, both NMIBC and MIBC, is a major source of morbidity and mortality among urinary tract malignancies worldwide. Patients are at substantial risk for recurrence and progression, even after complete surgical resection. Reliable prognostic tools are critically needed to recognize patients who are at the highest risk for progression so that clinical intervention can be carried out in advance. In this study, we established a platform called UBC-PD-L1 for predicting the prognosis of BLCA based on U-BCCs, which may help in the early identification of patients who tend to relapse and progress by non-invasive means. In addition,

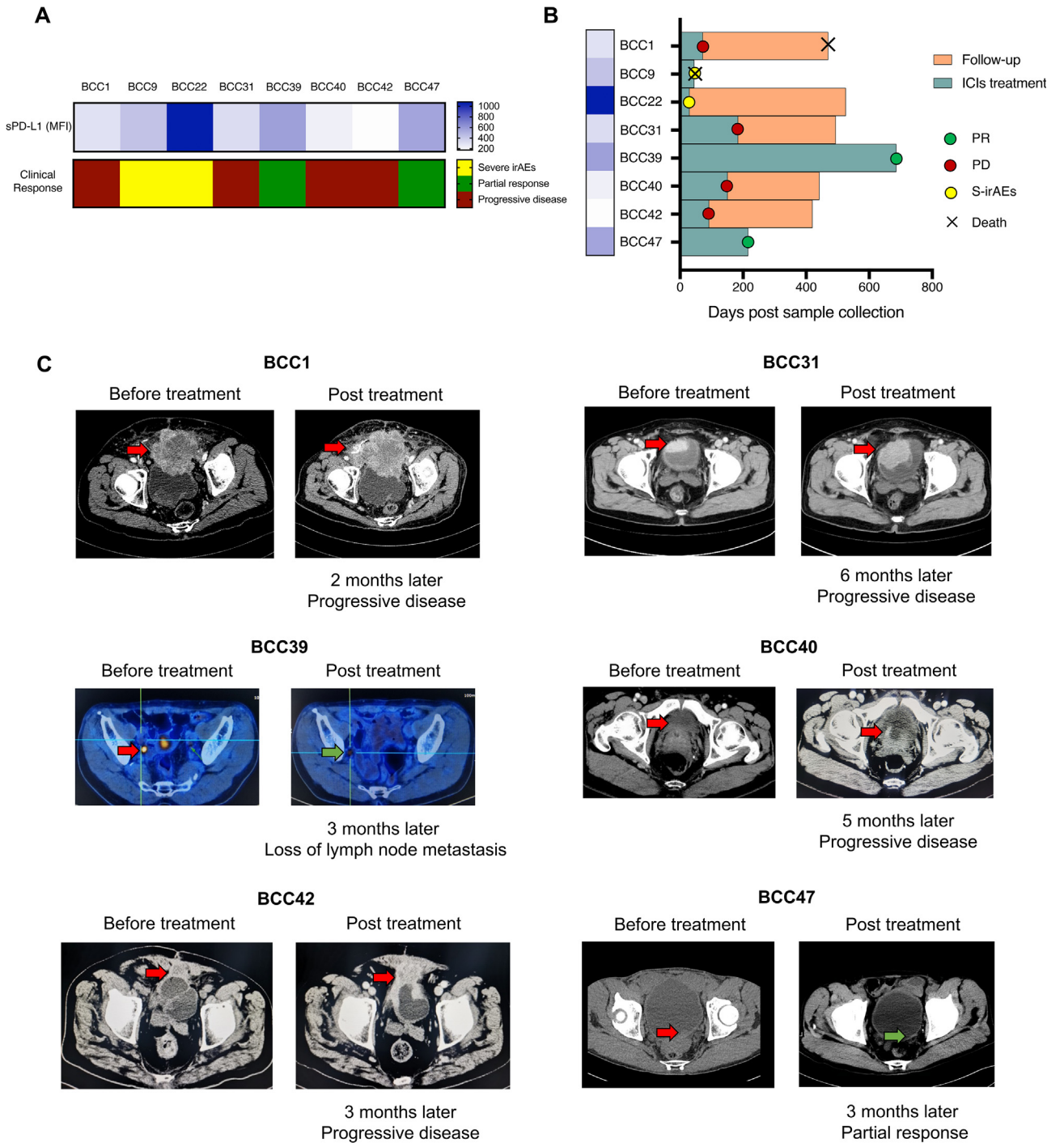

Figure 4 UBC-PD-L1 can predict the ICI response of BLCA. **(A)** The heatmap. of sPD-L1 expression levels of U-BCCs and corresponding clinical ICI response of patients. The upper row is the sPD-L1 expression levels detected by FCM in U-BCCs. The lower row is the patients' ICI clinical response: red indicate progressive disease, green indicate partial response, yellow indicate severe irAEs after ICI treatment. **(B)** Swimmer plot of treatment duration, ICI response, and clinical outcome. PR, partial response; PD, progressive disease; S-irAEs, severe immune-related adverse events. **(C)** The CT and PET-CT of the BCC1, BCC31, BCC39, BCC40, BCC42 and BCC47 patients before and after ICI treatment.

the UBC-PD-L1 may also aid in distinguishing patients who are most suitable for ICI treatment, further improving the efficiency of the clinical ICI treatment.

It has been reported that insensitivity to IFN-γ may contribute to tumor development and progression.[21] These prior data suggest that the lack of responsiveness of tumor cells to IFN-γ signaling due to impairment of the IFN-γ receptor or disruption of related pathways by various mediated mechanisms, which ultimately results in cancer development or progression.[22] As one of the downstream

factors of the signaling pathway, the change of PD-L1 expression level after IFN-γ stimulation was considered among the representation of the relative final manifestation. The Kaplan—Meier survival analysis indeed revealed that patients with high sPD-L1 demonstrated better survival. Based on transcriptome analysis, we found that BCCs with low sPD-L1 exhibited ECM and collagen downregulation, and reduction of cell—cell adhesion. ECM is a major component of the tumor microenvironment and serves not only as an anchor for epithelial cells to surrounding connective tissue but also as a significant barrier to epithelial cell migration.[23] Collagen is the most significant component of the ECM. The ECM can serve as binding sites, controlling the adhesion and movement of cells.[24] These all suggested that the low sPD-L1 BCCs are more likely to migrate and promote tumor progression. Previous studies reported that the immune surveillance of tumor cells drives alteration of the antigen processing and presentation pathways to evade detection.[25] Evasion of the immune response is a significant event during tumor development and progression. Compared to BCCs with high sPD-L1, BCCs with low sPD-L1 were more likely to evade the immune system due to the downregulation of positive regulation of the immune system process and antigen processing, foreshadowing the progress of the tumor.

Bladder cancer is often histologically heterogeneous within a given patient.[26] Our study showed that different BCCs have different PD-L1 expression and sensitivity to IFN-γ, and this diversity exists not only between tumor cells from different patients but also between subclones in tumor cells from the same patient. This further proved that the U/T-BCCs we cultured did retain the remarkable characteristics of tumor heterogeneity in BLCA. Previous studies have shown that urine from BLCA patients can provide an abundance of information related to their tumor status.[27—29] We also had demonstrated that urine-derived bladder cancer cells could recapitulate the broad histopathological and molecular spectrum of parental tumor tissues.[13] In this study, of major interest is our finding that U-BCCs have similar or even better prognostic value. The higher level of MKI67 expression on U-BCCs compared with T-BCCs in the same patient might suggest the higher malignant proliferative capacity of U-BCCs. Considering the intratumoral heterogeneity, U-BCCs may be a more dominant clone, which may partly explain its better prognostic value. Next, we will further identify the biological characteristics of U-BCCs and their roles during disease processes, in an attempt to provide new insights into the pathogenesis and development of bladder cancer and the possible therapeutic interventions.

Accumulating evidence from both preclinical and clinical studies mostly indicates that the pathological assessment of PD-L1 levels in tumor tissues currently used clinically is not a satisfactory predictor of anti-PD-1/PD-L1 treatment outcomes.[30] It has been reported that glycosylation of PD-L1 may render its polypeptide antigens inaccessible to PD-L1 antibodies, which may lead to inaccurate IHC readouts in some patient samples.[31] We demonstrated above that BC-PD-L1 can avoid the structural hindrance attributed to heavy glycosylation and provide a more accurate method for quantifying membrane PD-L1 expression. We speculate that sPD-L1 represents the sensitivity of tumor cells to the immune environment *in vivo*, at least to some extent. Ultra-high sPD-L1 may indicate ultra-sensitivity to the immune system, which might induce severe irAEs. Ultra-low sPD-L1 may indicate the immune inertia of the tumor and result in a lack of response to immunotherapy. Moderate sPD-L1 suggests sensitivity to the immune system, and immune activation induced by ICIs treatment can lead to high sPD-L1, further promoting ICIs response, and thereby forming a virtuous cycle. More importantly, due to the convenient and non-invasive method to obtain urine samples, UBC-PD-L1 is not only feasible for clinical translation, but also more likely to achieve real-time dynamic monitoring during treatment.

In conclusion, we established a novel, convenient PD-L1 dynamic detection platform based on U/T-BCCs. We demonstrated that UBC-PD-L1 can be used as a potential prognostic tool for clinical application in BLCA management, including the prediction of ICIs response. As a urine-based, non-invasive model, it is proved to be more convenient and practicable for BLCA patients, especially advanced patients, underscoring its significant potential for future clinical application in precision medicine.

Author contributions

Jiaqi Wang: Conceptualization, Methodology, Validation, Formal analysis, Writing - Original Draft, Funding acquisition; Jiying Zhu: Methodology, Validation, Formal analysis; Junchi Hu: Software, Formal analysis; Ziruoyu Wang: Software, Formal analysis; Xiaobo Wang: Methodology, Validation; Jianbo Pan: Software, Formal analysis; Yiwei Chu: Conceptualization, Supervision; Zengxia Li: Conceptualization, Supervision; Wei Jiang: Conceptualization, Supervision; Chunmin Liang: Supervision; Jun Hou: Formal analysis, Resources; Jianming Guo: Conceptualization, Supervision, Resources; Yongjun Dang: Conceptualization, Supervision, Resources, Writing - Review & Editing, Funding acquisition; Shuai Jiang: Conceptualization, Supervision, Resources, Writing - Review & Editing, Funding acquisition.

Conflict of interests

The authors disclose no potential conflict of interests.

Funding

This work was supported by the National Natural Science Foundation of China (No. 82073413 to S.J.), the Clinical and Research Fund of Wu Jieping Medical Foundation (No. 320.6750.2020-01-12 to S.J.), the National Natural Science Foundation of China (No. 22137002 to Y.D.), and the China Postdoctoral Science Foundation (No. 2020TQ0068 to J.W.).

Acknowledgements

We would like to thank Mrs. Yijing Zhu for her help in clinical sample collection.

Appendix A. Supplementary data

Supplementary data to this article can be found online at https://doi.org/10.1016/j.gendis.2022.10.022.

References

1. Berdik C. Unlocking bladder cancer. *Nature*. 2017;551(7679):S34—S35.
2. Christensen E, Birkenkamp-Demtröder K, Sethi H, et al. Early detection of metastatic relapse and monitoring of therapeutic efficacy by ultra-deep sequencing of plasma cell-free DNA in patients with urothelial bladder carcinoma. *J Clin Oncol*. 2019;37(18):1547—1557.
3. Patel VG, Oh WK, Galsky MD. Treatment of muscle-invasive and advanced bladder cancer in 2020. *CA A Cancer J Clin*. 2020;70(5):404—423.
4. Tran L, Xiao JF, Agarwal N, et al. Advances in bladder cancer biology and therapy. *Nat Rev Cancer*. 2021;21(2):104—121.
5. Lenis AT, Lec PM, Chamie K, et al. Bladder cancer: a review. *JAMA*. 2020;324(19):1980—1991.
6. Ignatiadis M, Sledge GW, Jeffrey SS. Liquid biopsy enters the clinic - implementation issues and future challenges. *Nat Rev Clin Oncol*. 2021;18(5):297—312.
7. Chauhan PS, Chen K, Babbra RK, et al. Urine tumor DNA detection of minimal residual disease in muscle-invasive bladder cancer treated with curative-intent radical cystectomy: a cohort study. *PLoS Med*. 2021;18(8):e1003732.
8. Chen X, Zhang J, Ruan W, et al. Urine DNA methylation assay enables early detection and recurrence monitoring for bladder cancer. *J Clin Invest*. 2020;130(12):6278—6289.
9. Dudley JC, Schroers-Martin J, Lazzareschi DV, et al. Detection and surveillance of bladder cancer using urine tumor DNA. *Cancer Discov*. 2019;9(4):500—509.
10. Valenberg FJPV, Hiar AM, Wallace E, et al. Prospective validation of an mRNA-based urine test for surveillance of patients with bladder cancer. *Eur Urol*. 2019;75(5):853—860.
11. Bao H, Bi H, Zhang X, et al. Artificial intelligence-assisted cytology for detection of cervical intraepithelial neoplasia or invasive cancer: a multicenter, clinical-based, observational study. *Gynecol Oncol*. 2020;159(1):171—178.
12. Lebret T, Pignot G, Colombel M, et al. Artificial intelligence to improve cytology performances in bladder carcinoma detection: results of the VisioCyt test. *BJU Int*. 2022;129(3):356—363.
13. Jiang S, Wang J, Yang C, et al. Continuous culture of urine-derived bladder cancer cells for precision medicine. *Protein Cell*. 2019;10(12):902—907.
14. Saeed K, Rahkama V, Eldfors S, et al. Comprehensive drug testing of patient-derived conditionally reprogrammed cells from castration-resistant prostate cancer. *Eur Urol*. 2017;71(3):319—327.
15. Kim D, Langmead B, Salzberg SL. HISAT: a fast spliced aligner with low memory requirements. *Nat Methods*. 2015;12(4):357—360.
16. Kluin RJC, Kemper K, Kuilman T, et al. XenofilteR: computational deconvolution of mouse and human reads in tumor xenograft sequence data. *BMC Bioinf*. 2018;19(1):366.
17. Kovaka S, Zimin AV, Pertea GM, et al. Transcriptome assembly from long-read RNA-seq alignments with StringTie2. *Genome Biol*. 2019;20(1):278.
18. Love MI, Huber W, Anders S. Moderated estimation of fold change and dispersion for RNA-seq data with DESeq2. *Genome Biol*. 2014;15(12):550.
19. Wu T, Hu E, Xu S, et al. clusterProfiler 4.0:a universal enrichment tool for interpreting omics data. *Innovation*. 2021;2(3):100141.
20. Väremo L, Nielsen J, Nookaew I. Enriching the gene set analysis of genome-wide data by incorporating directionality of gene expression and combining statistical hypotheses and methods. *Nucleic Acids Res*. 2013;41(8):4378—4391.
21. Mandai M, Hamanishi J, Abiko K, et al. Dual faces of IFNγ in cancer progression: a role of PD-L1 induction in the determination of pro- and antitumor immunity. *Clin Cancer Res*. 2016;22(10):2329—2334.
22. Zaidi MR, Merlino G. The two faces of interferon-γ in cancer. *Clin Cancer Res*. 2011;17(19):6118—6124.
23. Cox TR. The matrix in cancer. *Nat Rev Cancer*. 2021;21(4):217—238.
24. Pietilä EA, Gonzalez-Molina J, Moyano-Galceran L, et al. Co-evolution of matrisome and adaptive adhesion dynamics drives ovarian cancer chemoresistance. *Nat Commun*. 2021;12(1):3904.
25. Reeves E, James E. Antigen processing and immune regulation in the response to tumours. *Immunology*. 2017;150(1):16—24.
26. Lindskrog SV, Prip F, Lamy P, et al. An integrated multi-omics analysis identifies prognostic molecular subtypes of non-muscle-invasive bladder cancer. *Nat Commun*. 2021;12(1):2301.
27. Chen A, Fu G, Xu Z, et al. Detection of urothelial bladder carcinoma via microfluidic immunoassay and single-cell DNA copy-number alteration analysis of captured urinary-exfoliated tumor cells. *Cancer Res*. 2018;78(14):4073—4085.
28. Husain H, Melnikova VO, Kosco K, et al. Monitoring daily dynamics of early tumor response to targeted therapy by detecting circulating tumor DNA in urine. *Clin Cancer Res*. 2017;23(16):4716—4723.
29. Lotan Y, Black PC, Caba L, et al. Optimal trial design for studying urinary markers in bladder cancer: a collaborative review. *Eur Urol Oncol*. 2018;1(3):223—230.
30. Rimm DL, Han G, Taube JM, et al. A prospective, multi-institutional, pathologist-based assessment of 4 immunohistochemistry assays for PD-L1 expression in non-small cell lung cancer. *JAMA Oncol*. 2017;3(8):1051—1058.
31. Lee HH, Wang YN, Xia W, et al. Removal of N-linked glycosylation enhances PD-L1 detection and predicts anti-PD-1/PD-L1 therapeutic efficacy. *Cancer Cell*. 2019;36(2):168—178.e4.